Helmholtz-Zentrum Dresden-Rossendorf (HZDR)

HELMHOLTZ ZENTRUM
DRESDEN ROSSENDORF

Antiferromagnetic resonance in the cubic iridium hexahalides $(NH_4)_2IrCl_6$ and K_2IrCl_6

Bhaskaran, L.; Ponomaryov, O.; Wosnitza, J.; Khan, N.; Tsirlin, A. A.; Zhitomirsky, M. E.; Zvyagin, S.;

Originally published:

November 2021

Physical Review B 104(2021), 184404

DOI: https://doi.org/10.1103/PhysRevB.104.184404

Perma-Link to Publication Repository of HZDR:

https://www.hzdr.de/publications/Publ-33336

Release of the secondary publication based on the publisher's specified embargo time.

Antiferromagnetic resonance in the cubic iridium hexahalides $(NH_4)_2IrCl_6$ and K_2IrCl_6

L. Bhaskaran,[1,*] A. N. Ponomaryov,[1,†] J. Wosnitza,[1,2] N. Khan,[3] A. A. Tsirlin,[3] M. E. Zhitomirsky,[4] and S. A. Zvyagin[1,‡]

[1]*Dresden High Magnetic Field Laboratory (HLD-EMFL) and Würzburg-Dresden Cluster of Excellence ct.qmat, Helmholtz-Zentrum Dresden-Rossendorf, 01328 Dresden, Germany*

[2]*Institut für Festkörper- und Materialphysik, TU Dresden, 01062 Dresden, Germany*

[3]*Experimental Physics VI, Center for Electronics Correlations and Magnetism, Institute of Physics, University of Augsburg, 86135 Augsburg, Germany*

[4]*University Grenoble Alpes, Grenoble INP, CEA, IRIG, PHELIQS, 38000 Grenoble, France*

(Received 19 July 2021; revised 4 October 2021; accepted 11 October 2021; published 2 November 2021)

We report on high-field electron spin resonance studies of two iridium hexahalide compounds $(NH_4)_2IrCl_6$ and K_2IrCl_6. In the paramagnetic state, our measurements reveal isotropic g factors $g = 1.79(1)$ for the Ir^{4+} ions, in agreement with their cubic symmetries. Most importantly, in the magnetically ordered state, we observe two magnon modes with zero-field gaps of 11.3 and 14.2 K for $(NH_4)_2IrCl_6$ and K_2IrCl_6, respectively. Based on that and using linear spin-wave theory, we estimate the nearest-neighbor exchange couplings and anisotropic Kitaev interactions $J_1/k_B = 10.3$ K, $K/k_B = 0.7$ K for $(NH_4)_2IrCl_6$, and $J_1/k_B = 13.8$ K, $K/k_B = 0.9$ K for K_2IrCl_6, revealing the nearest-neighbor Heisenberg coupling as the leading interaction term, with only a weak Kitaev anisotropy.

DOI: 10.1103/PhysRevB.104.184404

Transition-metal compounds with partly filled $4d$ and $5d$ orbitals have recently attracted enormous attention as promising candidates for realizing novel magnetic phenomena, emerging from the interplay between crystal-field effects and spin-orbit interactions [1–3]. In particular, honeycomb magnets with $j_{\text{eff}} = \frac{1}{2}$ moments and bond-anisotropic Kitaev interactions have come under extensive scrutiny due to the possible realization of quantum spin liquid states, characterized by unusual spin dynamics with fractionalized Majorana fermions and flux excitations [4–8].

While the majority of experimental and theoretical studies remains focused on honeycomb materials as the most promising platform for the Kitaev interaction [9–11], there is also a significant interest in detecting anisotropic exchange terms (including the Kitaev interaction) in Ir^{4+} compounds with structures distinct from the honeycomb geometry [12–17]. However, most of the nonhoneycomb iridates studied over the last decade still evade detailed spectroscopic characterization with an unambiguous experimental determination of their interaction parameters. In particular, the absence of large single crystals as well as the notoriously strong neutron absorption by Ir atoms (which is of crucial importance for inelastic neutron scattering studies) and the insufficient energy resolution (in case of resonant inelastic x-ray scattering, RIXS) have often hindered the experimental access to relevant magnetic excitations.

Here we focus on two compounds from the family of Ir^{4+} antifluorites [18–21], $(NH_4)_2IrCl_6$ and K_2IrCl_6, that have been recently revisited by crystallographic and thermodynamic studies [22–24]. These compounds feature Ir^{4+} ions arranged on a face-centered cubic (fcc) lattice with four sublattices [Fig. 1(a)] and distinct long-range superexchange pathways mediated by the covalently bonded halogen ions [Fig. 1(b)]. The presence of possible frustration in fcc lattices is interesting in its own right as it shows an intricate competition of magnetic ground states, even in the absence of Kitaev or any other exchange anisotropy [25–27]. In contrast to many other iridates, these compounds are available as relatively large single crystals amenable to laboratory spectroscopic probes, featuring a cubic symmetry of the molecule that not only ensures the spin-orbit-coupled $j_{\text{eff}} = \frac{1}{2}$ state of the Ir^{4+} ions, but also restricts the number of relevant interaction parameters.

In the following we present electron spin resonance (ESR) studies of $(NH_4)_2IrCl_6$ and K_2IrCl_6, revealing the presence of two gapped magnon modes in each of the compounds. Employing linear spin-wave-theory calculations, we estimate the spin-Hamiltonian parameters and, consequently, establish the main interaction terms.

Single crystals of $(NH_4)_2IrCl_6$ and K_2IrCl_6 were grown from solutions prepared by dissolving commercially available powders (Alfa Aesar) in deionized water and keeping the solutions at 60 °C for several days. The resulting crystals had well-defined hexagonal (111) faces and sizes of ~2–3 mm^3. Magnetization measurements revealed magnetic ordering transitions at 2.15 K for $(NH_4)_2IrCl_6$ and 3.1 K for K_2IrCl_6, in agreement with previous studies [20,22,23,28].

*l.bhaskaran@hzdr.de

†Present address: Institute of Radiation Physics, Helmholtz-Zentrum Dresden-Rossendorf, 01328 Dresden, Germany.

‡s.zvyagin@hzdr.de

 ©2021 American Physical Society

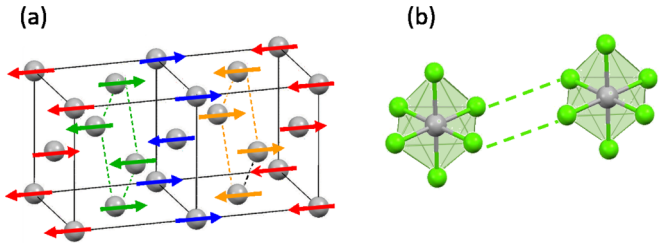

FIG. 1. (a) Schematic view of the type-III antiferromagnetic spin structure of the $IrCl_6$ fcc lattice with four sublattices. Spins belonging to different sublattices are shown in red, green, blue, and orange colors. (b) Schematic representation of nearest-neighbor Cl^--mediated superexchange pathways across the parallel edges of the octahedra formed by chlorine atoms. The Ir ions are shown in gray while the Cl ions are in green color.

High-field electron spin resonance (ESR) measurements were performed employing a transmission-type ESR spectrometer (similar to that described in Ref. [29]), in magnetic fields up to 16 T. Measurements were done in the frequency range of 60–400 GHz, using a set of VDI microwave-chain radiation sources (product of Virginia Diodes, Inc., USA). An InSb hot-electron bolometer (QMC Instruments Ltd., UK) was used to record the spectra. We measured single crystals in the Faraday configuration with magnetic field $H \parallel [111]$ and in the Voigt configuration with $H \perp [111]$. For the powder samples we confined the specimens by a binding agent such as high vacuum grease. The powders were obtained by crushing single crystals to ensure consistency between single-crystal and powder measurements. The stable free-radical molecule DPPH (2,2-diphenyl-1-picrylhydrazyl) was used as a frequency-field marker.

ESR is traditionally recognized as a powerful tool to probe crystal-field effects in solids. A very sensitive test of the presence of noncubic distortions in covalently bound $[IrCl_6]^{2-}$ complexes is provided by a g-factor anisotropy [18]. In Fig. 2 we show powder and single-crystal spectra obtained for $(NH_4)_2IrCl_6$ (a) and K_2IrCl_6 (b) at a temperature of 50 K. Both powder spectra were fit using a Lorentzian function with $g = 1.79(1)$, and linewidths of 0.93 and 1.23 T for $(NH_4)_2IrCl_6$ and K_2IrCl_6, respectively. These parameters perfectly agree with the simulation results for the single crystals along both $H \parallel [111]$ and $H \perp [111]$, revealing isotropic paramagnetic g factors, and thus evidencing the cubic symmetry for both compounds. The reduction of the g factor from the free-spin value ($g = 2$) can be attributed to the covalent nature of the Ir and Cl bonds [30,31]. Large covalency of the Ir^{4+} halides was indeed confirmed by recent RIXS studies [24], detecting also minor deviations from the $j_{\text{eff}} = \frac{1}{2}$ state [23], despite the absence of any macroscopic symmetry lowering [22].

Upon cooling, the ESR spectra for $H \parallel [111]$ exhibit significant broadening, evidencing enhancement of magnetic correlations, with the maximum in the vicinity of T_N (Figs. 3 and 4). On further decreasing the temperature, the ESR linewidth rapidly decreases, revealing the onset of long-range ordering below T_N. This transition into the ordered state also results in a pronounced low-temperature shift of the ESR field positions.

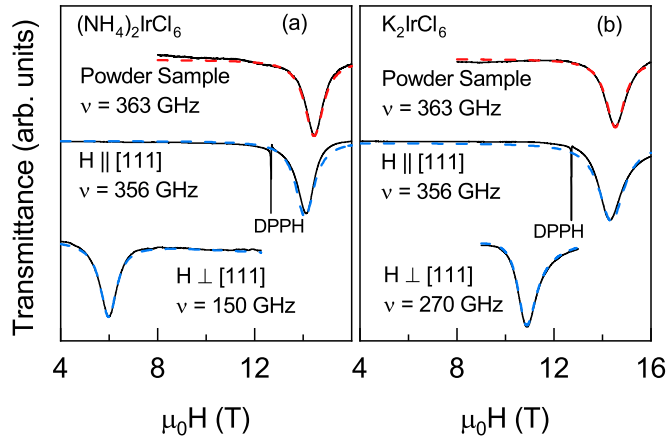

FIG. 2. Normalized ESR spectra measured in single-crystalline ($H \parallel [111]$ and $H \perp [111]$) and powder samples of (a) $(NH_4)_2IrCl_6$ and (b) K_2IrCl_6 at 50 K. The spectra are offset for clarity. Lorentzian fits to the powder sample are shown by the dashed red lines, while simulation of the single-crystal spectra are shown by the dashed blue lines.

Two antiferromagnetic resonance (AFMR) modes A_1 and A_2 were observed in the magnetically ordered state (Figs. 5 and 7). Selected AFMR spectra measured at 1.5 K with magnetic field applied along the [111] direction are shown in Fig. 6 for $(NH_4)_2IrCl_6$ and in the inset of Fig. 7 for K_2IrCl_6.

The frequency-field dependencies of the modes A_1 and A_2 can be described using the equation

$$h\nu = \Delta \pm g_{\text{eff}} \mu_B B, \tag{1}$$

where h is the Planck constant, ν represents the excitation frequency, g_{eff} is the effective g factor, and μ_B is the Bohr magneton. From this linear fit we obtain the zero-field magnon gaps $\Delta = 235 \pm 10$ and 295 ± 10 GHz (which correspond to 11.3 and 14.2 K; $g_{\text{eff}} = 0.8$) for $(NH_4)_2IrCl_6$ and K_2IrCl_6, respectively. For both materials, mode A_1 shows a linear increase in the resonance-field position, while some deviation from the linear dependence was observed for mode A_2 in high

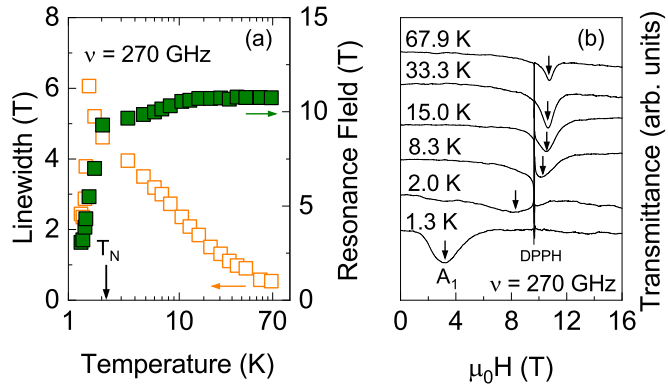

FIG. 3. (a) Temperature dependence of the resonance field (closed squares) and linewidth (open squares) measured in $(NH_4)_2IrCl_6$ at 270 GHz. (b) Examples of normalized ESR spectra recorded at 270 GHz and different temperatures. The spectra are offset for clarity. Magnetic field is applied along the [111] direction.

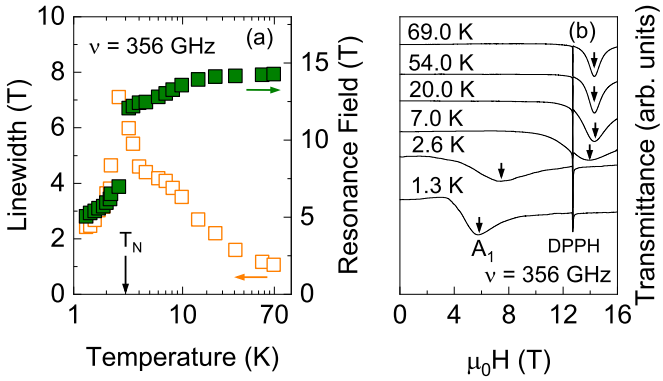

FIG. 4. (a) Temperature dependence of the resonance field (solid squares) and linewidth (open squares) measured in K_2IrCl_6 at 356 GHz. (b) Examples of normalized ESR spectra recorded at 356 GHz and different temperatures. The spectra are offset for clarity. Magnetic field is applied along the [111] direction.

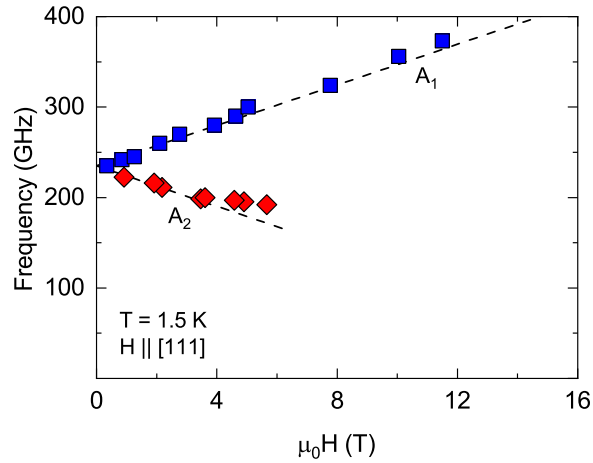

FIG. 5. Frequency-field diagram of ESR excitations in $(NH_4)_2IrCl_6$ measured at 1.5 K with magnetic field applied parallel to the [111] direction. The dashed lines represent linear fits using Eq. (1).

fields. Noticeably, the mode A_2 disappears above ~6 T. This field corresponds to a field-induced transition reported for K_2IrCl_6 [32], whereas in $(NH_4)_2IrCl_6$ the changes in applied field appear to be limited to a domain repopulation wherein the number of domains with magnetic moments oriented perpendicular to the applied field increases [33].

A general form of spin-spin interactions in magnetic systems with an fcc crystal structure was discussed by several authors [13,22,34,35]. Apart from the Heisenberg exchange, it includes symmetry-allowed anisotropic terms typical for materials with strong spin-orbit coupling. According to an *ab initio* calculation [22] two strongest spin-spin interactions in $(NH_4)_2IrCl_6$ and K_2IrCl_6 are the Heisenberg exchange $J_1 > 0$ and the Kitaev interaction $K > 0$ for the nearest-neighbor (nn) pairs of Ir ions. In addition, a weak next-nearest-neighbor (nnn) exchange $J_2 > 0$ is necessary to explain the experimentally observed type-III antiferromagnetic order [36]. Accordingly, we consider the following Hamiltonian for effective $S = 1/2$ moments of iridium ions:

$$\hat{\mathcal{H}} = \sum_{\langle ij \rangle}^{\text{nn}} \left(J_1 \mathbf{S}_i \cdot \mathbf{S}_j + K S_i^{\gamma} S_j^{\gamma} \right) + J_2 \sum_{\langle ij \rangle}^{\text{nnn}} \mathbf{S}_i \cdot \mathbf{S}_j, \qquad (2)$$

where $\mathbf{S}_i$ and $\mathbf{S}_j$ are spin-1/2 operators at site i and j, respectively. In the anisotropic Kitaev term, γ is one of the cubic axes (x, y, z) that is orthogonal to a given bond.

The Heisenberg fcc antiferromagnet with only the nearest-neighbor interactions has highly degenerate classical ground states [37]. A small positive next-nearest-neighbor exchange J_2 lifts this degeneracy in favor of the type-III magnetic structure described by the propagation vector $\mathbf{Q} = (2\pi/a, \pi/a, 0)$ [38] [note that $\mathbf{Q}' = (0, \pi/a, 2\pi/a) = -\mathbf{Q} + \mathbf{G}$, where $\mathbf{G}$ is a reciprocal lattice vector]. In addition, the anisotropy $K > 0$ locks magnetic moments in the (0,1,0) direction:

$$\mathbf{S}_i = \sqrt{2}\, S \hat{\mathbf{y}} \cos(\mathbf{Q} \cdot \mathbf{r}_i \pm \pi/4). \qquad (3)$$

Together with two other equivalent $\mathbf{Q}$, obtained by permutation of $Q_{x,y,z}$, there are in total six domains for the type-III collinear structure.

Following a recent theoretical study of the excitation spectra in fcc antiferromagnets [26], we have performed linear spin-wave calculations for the Hamiltonian (2) with $J_2, K > 0$. The ESR response corresponds to long wavelength excitations with $\mathbf{k} \to 0$. Accordingly, the ESR spectrum is formed by two degenerate pairs of gapped magnons with the zero-field excitation energies:

$$\Delta_l = 2\sqrt{KJ_2}, \quad \Delta_u = 2\sqrt{4KJ_1 + 2K^2 + KJ_2}. \qquad (4)$$

Note that the size of the low-energy gap Δ_l is determined by both K and J_2, while the upper gap Δ_u depends mainly on the strength of the Kitaev interaction. Moreover, in the absence of K both gaps vanish, while at $J_2 \to 0$ they have substantially different magnitudes.

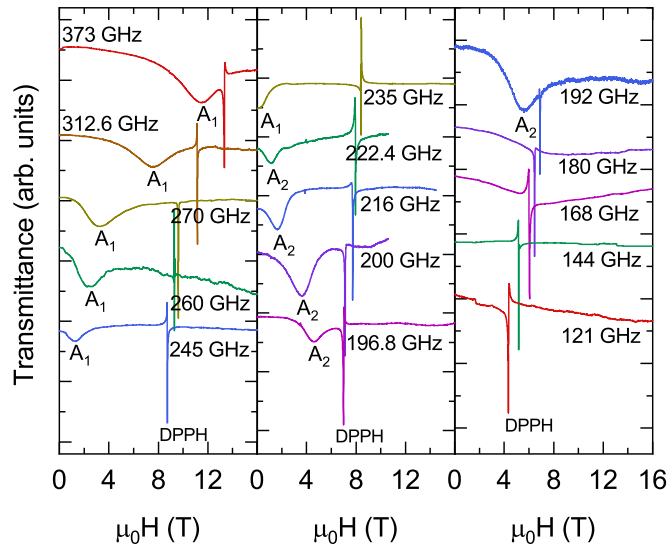

FIG. 6. Examples of normalized ESR spectra for $(NH_4)_2IrCl_6$ at different frequencies and $T = 1.5$ K with $H \parallel [111]$. The spectra are offset for clarity.

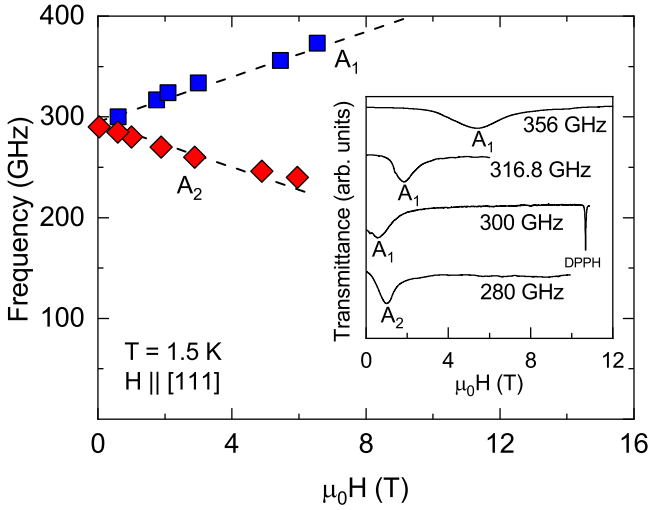

FIG. 7. Frequency-field diagram of ESR excitations in K_2IrCl_6 measured at 1.5 K with magnetic field applied parallel to the [111] direction. The dashed lines represent linear fits using Eq. (1). In the inset, examples of normalized ESR spectra for K_2IrCl_6 at different frequencies and $T = 1.5$ K with $H \parallel [111]$ are shown. The spectra are offset for clarity.

The next-nearest-neighbor isotropic exchange coupling was recently estimated from the *ab initio* calculation as $J_2/k_B \simeq 0.2$ K for both $(NH_4)_2IrCl_6$ and K_2IrCl_6 [22,33]. In addition, we use the expression for the Curie-Weiss temperature [39]

$$\theta_{CW} = 3J_1 + K + \tfrac{3}{2} J_2. \quad (5)$$

Experimental values for θ_{CW}/k_B are 32 K for $(NH_4)_2IrCl_6$ [33] and 42.6 K for K_2IrCl_6 [22]. They are obtained by fits to the magnetic-susceptibility data in the 100–400 K and 150–400 K range, respectively. The corresponding effective moment of 1.73 μ_B confirms that mostly the ground-state $j_{\text{eff}} = \frac{1}{2}$ doublet is occupied in this temperature range. Using Eqs. (4) and (5) we estimate $J_1/k_B = 10.3$ K and $K/k_B = 0.7$ K for $(NH_4)_2IrCl_6$, and $J_1/k_B = 13.8$ K and $K/k_B = 0.9$ K for K_2IrCl_6 ($K/J_1 \approx 6\%$–7%). The exchange coupling J_1 is stronger for K_2IrCl_6 compared to $(NH_4)_2IrCl_6$, due to the lattice parameter difference ($a = 9.77$ vs 9.87 Å [22,33], respectively), with the respective negative pressure reducing magnetic interactions in $(NH_4)_2IrCl_6$. It is worth noting that our experimental value of K is much smaller than the 5 K reported in Ref. [22]. This discrepancy may indicate the importance of Hund's coupling on the Cl ligand, an effect that has been neglected in the superexchange theory used in Ref. [22] and generally leads to a ferromagnetic contribution, which counteracts antiferromagnetic superexchange. Similar effects were previously reported in Cu^{2+} halides [40].

Using the parameters, as obtained above, the size of low-energy gaps was also estimated, yielding $\Delta_l/k_B \approx 1$ K. Our thorough search did not reveal the low-energy AFMR modes (note also that our ESR probe has a cut-off frequency limit of 60–70 GHz that is higher than the expected size of Δ_l). The absence of the low-energy ESR modes, which directly depends on J_2, may indicate, on the other hand, that the next-nearest-neighbor exchange in these compounds is very small. In such a case the quantum order-by-disorder effect can play a significant role in the Kitaev fcc antiferromagnets [41].

Summarizing, we presented systematic ESR studies of the two iridium hexahalide compounds $(NH_4)_2IrCl_6$ and K_2IrCl_6. In the paramagnetic state, our measurements reveal isotropic g factors $g = 1.79(1)$ for Ir^{4+} ions, confirming their cubic symmetries. By measuring the ESR spectra in the ordered state, we were able to determine the nearest-neighbor Heisenberg exchange J_1 and the Kitaev interaction K for both materials, revealing $K \ll J_1$. The intriguing possibility of the realization of the quantum order-by-disorder effect as well as details of the high-field behavior of magnetic excitations in these frustrated compounds deserves further experimental and theoretical studies.

This work was supported by the Deutsche Forschungsgemeinschaft, through ZV 6/2-2, the Würzburg-Dresden Cluster of Excellence on Complexity and Topology in Quantum Matter–*ct:qmat* (EXC 2147, Project No. 390858490), and SFB 1143, as well as by the HLD at HZDR, member of the European Magnetic Field Laboratory (EMFL). The work in Augsburg was supported by the Deutsche Forschungsgemeinschaft via the Project No. 107745057 (TRR80). M.E.Z. acknowledges financial support from ANR, France, Grant No. ANR-18-CE05-0023.

[1] W. Witczak-Krempa, G. Chen, Y. B. Kim, and L. Balents, Correlated quantum phenomena in the strong spin-orbit regime, Annu. Rev. Condens. Matter Phys. **5**, 57 (2014).

[2] J. G. Rau, E. K.-H. Lee, and H.-Y. Kee, Spin-orbit physics giving rise to novel phases in correlated systems: Iridates and related materials, Annu. Rev. Condens. Matter Phys. **7**, 195 (2016).

[3] G. Cao and P. Schlottmann, The challenge of spin–orbit-tuned ground states in iridates: A key issues review, Rep. Prog. Phys. **81**, 042502 (2018).

[4] A. Kitaev, Anyons in an exactly solved model and beyond, Ann. Phys. **321**, 2 (2006).

[5] G. Baskaran, S. Mandal, and R. Shankar, Exact Results for Spin Dynamics and Fractionalization in the Kitaev Model, Phys. Rev. Lett. **98**, 247201 (2007).

[6] G. Jackeli and G. Khaliullin, Mott Insulators in the Strong Spin-Orbit Coupling Limit: From Heisenberg to a Quantum Compass and Kitaev Models, Phys. Rev. Lett. **102**, 017205 (2009).

[7] O. Petrova, P. Mellado, and O. Tchernyshyov, Unpaired Majorana modes in the gapped phase of Kitaev's honeycomb model, Phys. Rev. B **88**, 140405(R) (2013).

[8] A. N. Ponomaryov, L. Zviagina, J. Wosnitza, P. Lampen-Kelley, A. Banerjee, J.-Q. Yan, C. A. Bridges, D. G. Mandrus, S. E.

Nagler, and S. A. Zvyagin, Nature of Magnetic Excitations in the High-Field Phase of α-$RuCl_3$, Phys. Rev. Lett. **125**, 037202 (2020).

[9] H. Takagi, T. Takayama, G. Jackeli, G. Khaliullin, and S. E. Nagler, Concept and realization of Kitaev quantum spin liquids, Nat. Rev. Phys. **1**, 264 (2019).

[10] S. M. Winter, A. A. Tsirlin, M. Daghofer, J. van den Brink, Y. Singh, P. Gegenwart, and R. Valenti, Models and materials for generalized Kitaev magnetism, J. Phys.: Condens. Matter **29**, 493002 (2017).

[11] A. A. Tsirlin and P. Gegenwart, Kitaev magnetism through the prism of lithium iridate, Phys. Status Solidi B 2100146 (2021).

[12] M. Becker, M. Hermanns, B. Bauer, M. Garst, and S. Trebst, Spin-orbit physics of $j = \frac{1}{2}$ Mott insulators on the triangular lattice, Phys. Rev. B **91**, 155135 (2015).

[13] A. M. Cook, S. Matern, C. Hickey, A. A. Aczel, and A. Paramekanti, Spin-orbit coupled $j_{\rm eff} = 1/2$ iridium moments on the geometrically frustrated fcc lattice, Phys. Rev. B **92**, 020417(R) (2015).

[14] S. Trebst, Kitaev materials, arXiv:1701.07056.

[15] A. A. Aczel, A. M. Cook, T. J. Williams, S. Calder, A. D. Christianson, G.-X. Cao, D. Mandrus, Y.-B. Kim, and A. Paramekanti, Highly anisotropic exchange interactions of $j_{\rm eff} = \frac{1}{2}$ iridium moments on the fcc lattice in La_2BIrO_6 (B = Mg, Zn), Phys. Rev. B **93**, 214426 (2016).

[16] A. A. Aczel, J. P. Clancy, Q. Chen, H. D. Zhou, D. Reig-i-Plessis, G. J. MacDougall, J. P. C. Ruff, M. H. Upton, Z. Islam, T. J. Williams, S. Calder, and J.-Q. Yan, Revisiting the Kitaev material candidacy of Ir^{4+} double perovskite iridates, Phys. Rev. B **99**, 134417 (2019).

[17] A. Revelli, C. C. Loo, D. Kiese, P. Becker, T. Fröhlich, T. Lorenz, M. Moretti Sala, G. Monaco, F. L. Buessen, J. Attig, M. Hermanns, S. V. Streltsov, D. I. Khomskii, J. van den Brink, M. Braden, P. H. M. van Loosdrecht, S. Trebst, A. Paramekanti, and M. Grüninger, Spin-orbit entangled $j = \frac{1}{2}$ moments in Ba_2CeIrO_6: A frustrated fcc quantum magnet, Phys. Rev. B **100**, 085139 (2019).

[18] J. H. E. Griffiths and J. Owen, Complex hyperfine structures in microwave spectra of covalent iridium compounds, Proc. R. Soc. London Ser. A **226**, 96 (1954).

[19] J. H. E. Griffiths, J. Owen, J. G. Park, and M. F. Partridge, Exchange interactions in antiferromagnetic salts of iridium. I. Paramagnetic resonance experiments, Proc. R. Soc. London Ser. A **250**, 84 (1959).

[20] A. H. Cooke, R. Lazenby, F. R. McKim, J. Owen, and W. P. Wolf, Exchange interactions in antiferromagnetic salts of iridium II. Magnetic susceptibility measurements, Proc. R. Soc. London Ser. A **250**, 97 (1959).

[21] E. A. Harris and J. Owen, The magnetic properties of three exchange coupled iridium ions, Proc. R. Soc. London Ser. A **289**, 122 (1965).

[22] N. Khan, D. Prishchenko, Y. Skourski, V. G. Mazurenko, and A. A. Tsirlin, Cubic symmetry and magnetic frustration on the fcc spin lattice in K_2IrCl_6, Phys. Rev. B **99**, 144425 (2019).

[23] D. Reig-i-Plessis, T. A. Johnson, K. Lu, Q. Chen, J. P. C. Ruff, M. H. Upton, T. J. Williams, S. Calder, H. D. Zhou, J. P. Clancy, A. A. Aczel, and G. J. MacDougall, Structural, electronic, and magnetic properties of nearly ideal $J_{\rm eff} = \frac{1}{2}$ iridium halides, Phys. Rev. Mater. **4**, 124407 (2020).

[24] N. Khan, D. Prishchenko, M. H. Upton, V. G. Mazurenko, and A. A. Tsirlin, Towards cubic symmetry for Ir^{4+}: Structure and magnetism of the antifluorite K_2IrBr_6, Phys. Rev. B **103**, 125158 (2021).

[25] M. E. Lines, Antiferromagnetism in the face-centred cubic lattice by a spin-wave method, Proc. R. Soc. London Ser. A **271**, 105 (1963).

[26] R. Schick, T. Ziman, and M. E. Zhitomirsky, Quantum versus thermal fluctuations in the fcc antiferromagnet: Alternative routes to order by disorder, Phys. Rev. B **102**, 220405(R) (2020).

[27] P. Balla, Y. Iqbal, and K. Penc, Degenerate manifolds, helimagnets, and multi-Q chiral phases in the classical Heisenberg antiferromagnet on the face-centered-cubic lattice, Phys. Rev. Res. **2**, 043278 (2020).

[28] C. A. Bailey and P. L. Smith, Specific heats of ammonium, potassium, and sodium chloroiridates, Phys. Rev. **114**, 1010 (1959).

[29] S. A. Zvyagin, J. Krzystek, P. H. M. van Loosdrecht, G. Dhalenne, and A. Revcolevschi, High-field ESR study of the dimerized-incommensurate phase transition in the spin-Peierls compound $CuGeO_3$, Physica B: Condens. Matter **346-347**, 1 (2004).

[30] K. W. H. Stevens and M. H. L. Pryce, On the magnetic properties of covalent XY_6 complexes, Proc. R. Soc. London Ser. A **219**, 542 (1953).

[31] J. H. M. Thornley, C. D. Lustig, and J. Owen, The magnetic properties of $(IrX_6)^{2-}$ complexes, J. Phys. C: Solid State **1**, 1024 (1968).

[32] M. Meschke, S. Marquardt, and K. Siemensmeyer, Field-induced phase transition in a type III fcc antiferromagnet: K_2IrCl_6, J. Magn. Magn. Mater **226**, 621 (2001).

[33] N. Khan, D. Khalyavin, P. Manuel, and A. A. Tsirlin (unpublished).

[34] B. Hälg and A. Furrer, Anisotropic exchange and spin dynamics in the type-I (-IA) antiferromagnets CeAs, CeSb, and USb: A neutron study, Phys. Rev. B **34**, 6258 (1986).

[35] I. Kimchi and A. Vishwanath, Kitaev-Heisenberg models for iridates on the triangular, hyperkagome, kagome, fcc, and pyrochlore lattices, Phys. Rev. B **89**, 014414 (2014).

[36] M. T. Hutchings and C. G. Windsor, The magnetic structure of K_2IrCl_6, Proc. Phys. Soc. **91**, 928 (1967).

[37] P. W. Anderson, Generalizations of the Weiss molecular field theory of antiferromagnetism, Phys. Rev. **79**, 705 (1950).

[38] Y. Yamamoto and T. Nagamiya, Spin arrangements in magnetic compounds of the rocksalt crystal structure, J. Phys. Soc. Jpn. **32**, 1248 (1972).

[39] N. W. Ashcroft and N. D. Mermin, *Solid State Physics* (Thomson Brooks/Cole, Boston, MA, 1976).

[40] S. Lebernegg, M. Schmitt, A. A. Tsirlin, O. Janson, and H. Rosner, Magnetism of CuX_2 frustrated chains (X = F, Cl, Br): Role of covalency, Phys. Rev. B **87**, 155111 (2013).

[41] F.-Y. Li, Y.-D. Li, Y. Yu, A. Paramekanti, and G. Chen, Kitaev materials beyond iridates: Order by quantum disorder and Weyl magnons in rare-earth double perovskites, Phys. Rev. B **95**, 085132 (2017).